Visualization of thermal plume using background-oriented schlieren based on phase-differences extraction of spatial fringe patterns

Margi Sasono[a]

[a]*Study Program of Physics, Ahmad Dahlan University, Yogyakarta, Indonesia*

Abstract

A specific technique is crucial for visualizing a thermal plume (gas) invisible. Mainly, the visualization uses the intrusive technique, disturbing the originality of the thermal plume. A background-oriented schlieren (BOS) optical technique alternatively offers a simple and non-intrusive visualization. However, the conventional BOS needs to be improved by accurate visualization. This paper proposes a new way of the BOS using a fringe patterns background with a spatial carrier frequency. The thermal plume modulates the phase of the background. A method similar to that in the communication field demodulates the phase, containing the physical information on the thermal plume, such as density or refractive index. The BOS has accurately been calibrated using a wedge prism. This way, the calibrated BOS has successfully visualized the thermal plume into phase and amplitude images. The proposed BOS has the potential to accurately measure the quantitative physical of the thermal plume or other transparent materials.

Keywords: Visualization; thermal; phase; demodulation; schlieren.

1. Introduction

A thermal plume (hot air rising) is a transparent gas invisible to the human eyes [1]. Hence, the visualization needs a specific technique. Nowadays, thermal plume visualization has encountered many applications, such as in gas leakage detection [2][3], exhaust plumes of rocket engines [4], chemical industrial [5], as well as in the areas of geophysics (geothermal) [6], atmospheric sciences [7], and many others. However, the visualization mainly uses intrusive methods, in which the pressure or temperature probe in the area testing can disturb the originality of the thermal plume.

Alternatively, a background-oriented schlieren (BOS) optical technique offers simple and non-intrusive visualization [8]. The optical setup of BOS technically requires only background patterns and a digital camera. The BOS visualization relies on the phenomenon of light refraction, occurred when the light enters the fluids (thermal plume) of a different density and the refractive index. The camera captures this light refraction, called the distorted background image (image distortion). A qualitative image of the thermal plume can be visualized by digitally comparing the distorted image to an undistorted image as a reference. Therefore, the BOS is a versatile tool to visualize fluids such as fluid flow [9], aerodynamics fields [10], the atmosphere [11], and shock waves [12]. Currently, the BOS can visualize the quantitative evaluation of the refractive index [13] and the density gradient in the fluids [14].

The image processing of the BOS relies on analyzing distorted patterns (image distortion) [8][15]. The BOS visualization strongly depends on the type of patterns used as the background. Therefore, the design of patterns plays an essential role in developing the BOS. Mainly, the background patterns use random dots and the digital image correlation (DIC) algorithm as the image processing technique [16]. However, the random dots can introduce an inhomogeneous distribution in the background plane [17] and can experience shape distortion due to the large density gradients of a medium [15]. In addition, the DIC algorithm tightly assumes the constant displacement pattern in the image distortion [17]. The violation of this condition can induce an inaccurate visualization.

This paper proposes a new way to visualize the thermal plume using the BOS technique. The proposed method uses a periodic fringe instead of a random dot pattern as a background. The fringe pattern behaves as a carrier spatial frequency (carrier image) that will be phase-modulated by the thermal plume, called the modulated image. The phase can be retrieved using phase demodulation, similar to the method used in the communication field [18]. Previously, research has shown that the phase demodulation method offers an accurate result, such as in the design of phase microscopy [19]. The method relies on the Hilbert Transform (HT) of the images [20], either the image distortion (modulated) or the reference (carrier image), as captured by a camera in the BOS experimental. The phase difference between the images contains the qualitative and quantitative visualization of the thermal plume. Thus, the developed BOS can offer high accuracy, fast, easy-to-use, and simplicity in visualizing the thermal plume or other transparent materials.

2. Materials and Methods

Technically, a BOS technique requires only a background and a camera unit as main components**.** Figure 1 shows the schematic diagram of the BOS experimental setup. A light source back-illuminates the background. The scheme places the background position at a distance $Z \gg f$ from the camera lens, where f is the focal length of a lens. In this way, the scheme allows the paraxial approximation or the propagation of parallel light rays from the background to the camera lens [8]. A hot object (thermal plume) in the test section, as shown in Fig.1, will produce a change in the refractive index (density) of the fluid (the air inside the test section) caused by the different temperatures. When the parallel light rays enter the test section, the optical path lengths will change and deflect toward the air with the higher density [21]. A digital camera records the light deflections into an image of a distorted background pattern (image distortion).

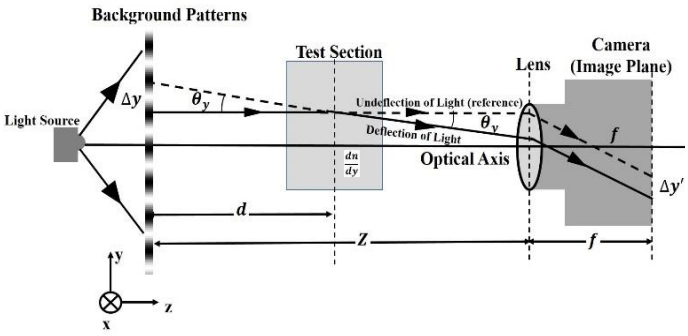

Fig. 1. The schematic diagram of a BOS experimental setup.

2.1. The BOS Principle based on Phase Demodulation

Referring to Fig.1, Fermat's principle mathematically reveals that the propagation of a light ray (along the z-axis) through an inhomogeneous medium with the refractive index variation as [22]

$$\frac{d^2y}{dz^2} = \frac{1}{n}\left(\frac{dn}{dy}\right) \tag{1}$$

where n is the refractive index of the surrounding medium and $\left(\frac{dn}{dy}\right)$ is the refractive index gradient (or spatial variation of the refractive index). Equation (1) relates the curvature of the refracted light ray to the magnitude of the refractive index gradient. Since the light ray deflection is a very small angle, integrating (1) gives in the angle of the y-component (θ_y) as

$$\theta_y = \frac{1}{n}\int\left(\frac{dn}{dy}\right)dz = \frac{\Delta y}{d} \tag{2}$$

where d is the distance between the thermal plume in the test section and the background, and Δy represents the displacement of the fringe pattern in the background plane. Thus, the angle deflection in (2) depends on the displacement of the fringe pattern (Δy), as indicated by the image distortion.

As captured by a camera, the background image has a periodic fringe pattern with a spatial carrier frequency. In the case of horizontal fringes (or the fringe pattern along the *x*-axis), the spatial carrier frequency is in the y-direction (υ_y). Mathematically, (3) describes the carrier intensity distribution after removing the background intensity (intensity with a low frequency) [23]as

$$I_{cr}(x,y) = I_o(x,y)\cos\left[(2\pi\upsilon_y)y\right] \tag{3}$$

where $I_{cr}(x,y)$ is the intensity at the position (x,y) or each pixel in the image plane, $I_0(x,y)$ is the intensity maximum or the modulation of the fringe patterns, υ_y is spatial carrier frequency along the y-axis, and (x,y) is spatial in the image plane. Equation (3) is the standard mathematical model for a two-dimensional (2-D) fringe pattern similar to the optical interferometer [24]. Modulating (3) will carry the desired phase information. The presence of a thermal plume will introduce the displacement of the fringe patterns and allow the phase-modulated intensity or image distortion in the BOS experimental. In this way, (3) changes into the modulated intensity as

$$I_m(x,y) = I_0\cos\left[\left(2\pi\upsilon_y\right)y + \varphi_m(x,y)\right] \tag{4}$$

where $\varphi_m(x,y)$ is the unknown modulating phase or phase variation of fringe patterns due to the thermal plume. Subtraction (4) from (3) gives the phase difference $\Delta\phi$ in proportion to the modulating phase $\varphi_m(x,y)$ and the displacement of the fringe pattern Δy as [23]

$$\Delta\varphi\,(x,y) = \varphi_m(x,y) = 2\pi\upsilon_y(\Delta y) \tag{5}$$

The main objective of phase demodulation is the extraction of the phase difference in (5) to estimate the physical information on the thermal plume.

This work uses the Hilbert Transform (HT) [24] for extracting the phase difference in (5). The HT operation transforms the real-valued intensity in (3) and (4) to the complex-valued intensity called an analytic signal (in terms of the signal theory), $Z(x,y)$, defined by [25]

$$Z(x,y) = Z_R(x,y) + iZ_{IM}(x,y) \tag{6}$$

where $Z_R(y)$ is the real-valued intensity, $i = \sqrt{-1}$ is the imaginer number, and $Z_{IM}(y)$ is the imaginer-valued intensity. Mathematically, the result of phase calculation using (6) is a wrapped phase (φ_{WR}) in the range $(-\pi, +\pi)$ as

$$\varphi_{WR}\,(x,y) = \arctan\left[\frac{Z_{IM}(x,y)}{Z_R(x,y)}\right] \tag{7}$$

The calculated phase in (7) requires an unwrapping process to obtain the absolute (actual) phase containing the physical information on the thermal plume. In detail, the literature [26][27] elucidates the algorithm for the unwrapping process. In addition, the absolute amplitude of analytic signal in (6) can also be obtained as

$$A_Z\,(x,y) = \sqrt{Z_R(x,y)^2 + Z_{IM}(x,y)^2} \tag{8}$$

where $\boldsymbol{A_Z\,(x,y)}$ is the absolute amplitude of an analytic signal. An amplitude image can be reconstructed using (8), containing information on the light intensity variation detected by the camera sensor.

2.2. Experiment Setup

This work uses a background with a black and white fringe pattern (fringe thickness is 1 mm) printed on 30 cm x 30 cm transparent materials. A white LED (Light Emitting Diode) panel back-illuminates the transparent materials to provide a light source. This pattern configures a periodic fringe pattern with a spatial carrier frequency or spatial period along the y-axis $p_y = 25$ pixels. The positioning of the background, the test section, and the camera in the setup refer to Fig.1. A digital camera used in this work is a model Hayear with an image resolution of 1800 pixels x 1920 pixels and a spatial resolution of 1.43 μm/pixel. The lens attached to the camera is a model Fujian with a focal length of $f = 50$ mm. Also, the camera provides a system connected to a personal computer (PC) for capturing and recording images. In operating the camera, the lens focuses on the background patterns. The position of the thermal plume (in the test section) is at a distance of $d = 500$ mm from the background (Fig.1).

The first step calibrates the BOS experimental by measuring the known angle deflection to validate the measurement results. This angle is determined as the measurement standard. This work uses a wedge prism 4 cm x 4 cm in size with an angle

deflection of 0.57°(refer to the manufacturer's manual sheets). The second step tests the calibrated BOS to visualize the thermal plume above a hot plate and an unstable candle flame in the test section. An electrical heater heats the circular plate of 10 cm diameter. During the experiment, the measured temperature of the hot plate was constant at 50 ℃. Referring to Fig.1, the plate surface (in the test section) is in the x-z plane and introduces a thermal plume along the y-axis. In addition, this work also visualizes the thermal plume above the unstable candle flame. A mini fan slowly runs to allow the blown air in the test section, generating the unstable flame of a candle. As a result, the thermal plume rises above the unstable flame. The camera captures all images of the thermal plume in the x-y plane (in the test section).

3. Results and Discussion

3.1. BOS Calibration

Firstly, the camera captures a photograph of a reference image (carrier image), as shown in Fig.2a. The placement of a wedge prism in the test section displaces the fringe patterns. The camera captures these displacements as a photograph of image distortion, as shown in Fig.2b. Visually, the fringe displacements appear in a single direction (y-direction), indicating uniformity. Optically, the homogeneity of the refractive index gradient in the wedge prism (indicated by arrow) produces a constant of the light deflection. As shown in Fig.2c, the intensity profiles (in the gray-level) along the white dashed line in both images (Fig.2a and Fig.2b) clearly show the phase difference. Hence the refractive index gradient of a wedge prism can modulate the phase of the reference image (carrier image).

The phase demodulation method using a Hilbert Transform (HT) can extract the phase difference and the absolute amplitude between both the images in Fig.2a (reference image) and Fig.2b (image distortion). The HT operation transforms the real-valued intensity in both images in a column-by-column manner, giving the complex-valued intensity. The calculation using (7) yields the wrapped phase images, and the unwrapping process converts them into unwrapped phase images. Subtracting the unwrapped phase of the image distortion from the reference image yields an image of phase difference, as shown in Fig.3a. The image in Fig.3a reveals the distribution of the desired phase differences and contains the physical information on a wedge prism. Applying (5) and (2) can convert the phase differences into the fringe displacements in the y-direction and the angles deflection of light, respectively. The image in Fig.3b represents the distribution of angles deflection in the area of a wedge prism (indicated by an arrow). As shown in Fig.3b, the area wedge prism visually appears homogeneous, indicating a constant of angles deflection. This result is convenient with the main optical characteristics of a wedge prism. By comparison in Fig.3a, the images are visually similar. This result confirms that the phase difference is proportional to the angle deflection.

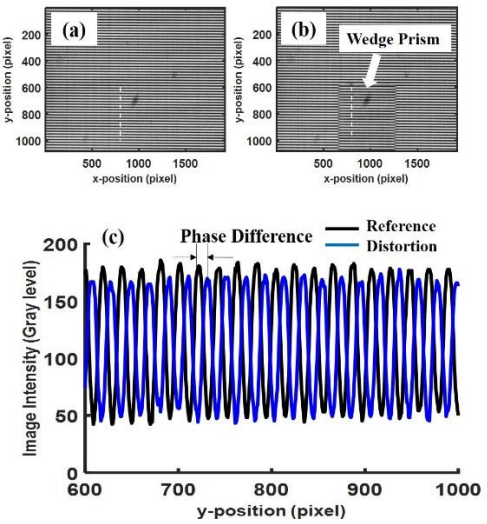

Fig. 2. Photograph of the background fringe patterns. (a) Reference image; (b) Image distortion due to the presence of a wedge prism in the test section; (c) The phase difference between both profiles of image intensity (in the gray level) along the white dashed line in both images (a) and (b).

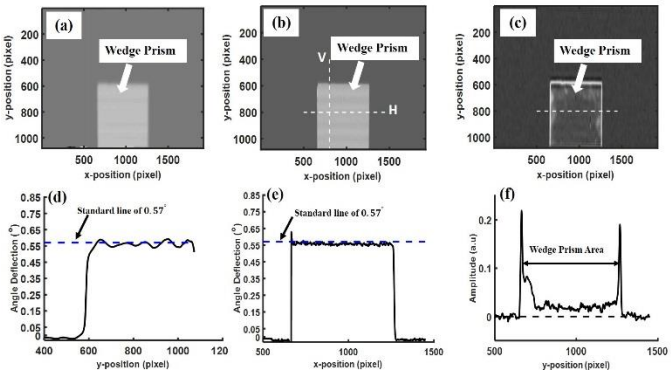

Fig. 3. Image reconstruction of a wedge prism using the BOS technique: (a) Phase image ; (b) Image of angle deflection; (c) Amplitude image; (d) Vertical (V) profile across the image in (b); (e) Horizontal (H) profile across the image in (b);(f) Horizontal amplitude profile across the image in (c) along the white dashed line.

The calibration process relies on the image profiles at a given data (along the white dashed line) in Fig.3b. The plot of the measured angles deflection versus the position (in the pixels unit) in Fig.3d and Fig.3e show the image profile of horizontal (H) and vertical (V), respectively. When the white dashed line across the area of a wedge prism, the curves rise and then tend to be flat to an angle of 0.57° (standard angle). These results show that all the deflection angles measured by the BOS experimental approach standard line angle of 0.57° (indicated by the blue dashed line).

The amplitude image of a wedge prism can be reconstructed using (8). The reconstructed image and the corresponding profile along a horizontal line are shown in Fig.3c and Fig.3f, respectively. The amplitude image (Fig.3c) describes the transmitted light intensity (in the arbitrary unit or a.u) detected by the camera sensor. Visually, the image tends to be nearly homogeneous except at the periphery of a wedge prism. The profile in Fig.3f represents the behaviour of the image intensity along a white dashed line in Fig.3c. As can be observed, the amplitude value in the area of a wedge prism tends to be almost identical to the value of the image background. This result confirms that the wedge prism has high transparency (less light

absorption) and is convenient as a phase object in the BOS calibration. It can be noted that the phase and amplitude images give a difference in characterizing the optical properties of a wedge prism.

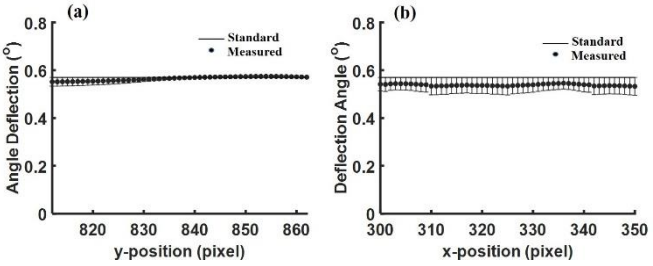

Fig. 4. Plot with error bars (taken only 50 data of curve flat in Fig.3d and Fig.3e) of the measured angle deflection in the area of a wedge prism using the BOS experimental : (a) The measured data in the vertical direction; (b) The measured data in the horizontal direction.

The process calibration evaluates the measurement accuracy by subtracting the measured angle data (only 50 data of the plat curve in Fig.3d and Fig.3e) from the standard angle, giving an error in measurements. Plot with error bars can represent the estimated (measured) angles deflection with the standard angle deviation (error in measurement) at each pixel in the image plane. As shown in Fig.4a and Fig.4b, the measured angle deflection spatially fluctuates around the standard line. The error bars on each data point indicate a closeness of measurement results with the standard angle of 0.57˚. Generally, all the deflection angle measured by the BOS experimental gives an error percentage of less than 5%, giving a measurement accuracy of the BOS experimental more than 95%.

3.2. Thermal plume of a hot plate

A circular plate was placed in the test section, as referred to in Fig.1. As in section 3.1, the camera first captures a reference image (carrier image) when the thermal plume is absent in the test section. The photograph of a reference image is shown in Fig.5a. An electrical heater heats the circular plate until it reaches a steady temperature of 50 ℃. The hot plate introduces the thermal plume (hot air rising) in the test section area. The camera captures a photograph of image distortion, as shown in Fig.5b. Visually, the fringe displacement in Fig.5b is not so visible. However, the image intensity profiles (in the gray-level), as shown in Fig.5c, along the white dashed line in both images (Fig.5a and Fig.5b), clearly show the phase difference. Thus, the thermal plume above the hot plate in the test section modulates the fringe patterns (modulation of the carrier image).

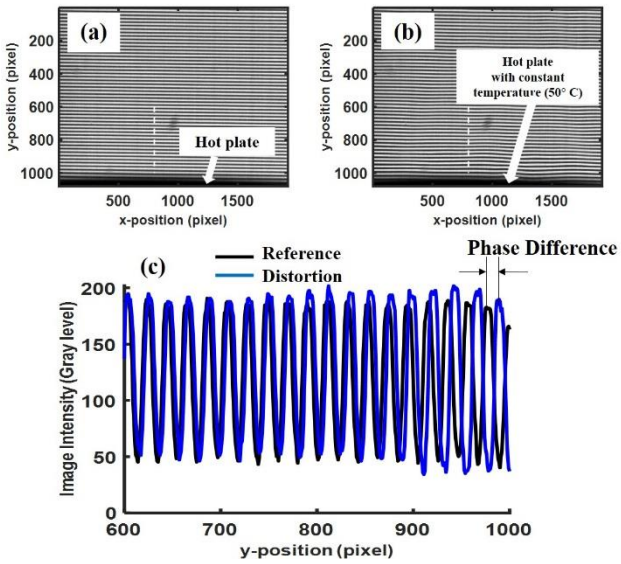

Fig. 5. Photograph of the background fringe patterns. (a) Reference image; (b) Image distortion due to the presence of a hot plate in the test section; (c) The phase difference between both profiles of image intensity (in the gray level) along the white dashed line in both images (a) and (b).

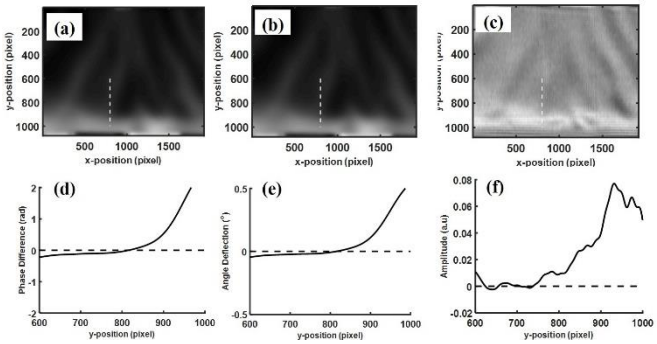

Fig. 6. The BOS visualization of the thermal plume in the case of a hot plate: (a) Phase (phase difference) image; (b) Image of angle deflection; (c) Amplitude image; (d) Phase profile along the white dashed line in the image (a); (e) Angle deflection profile along the white dashed line in the image (b); and (f) Amplitude profile along the white dashed line in the image (c).

The phase of photographs in Fig.5a and Fig.5b can be extracted using the HT operation. The extracted phases can be reconstructed into a phase (phase difference) image, as shown in Fig.6a. Furthermore, the reconstructed image of angle deflection is shown in Fig.6b. Visually, both images contain noise and tend to be dark. As can be observed, the image contrast indicates the presence of the thermal plume due to a hot plate in the test section. The brightness variation in the image describes the value of phase difference or the angle deflection, containing the physical information on density variation (refractive index gradient) in the thermal plume. The image profiles, as shown in Fig.6d and Fig.6e, along the white dashed line in the images (Fig.6a and Fig.6b), confirm this result. As can be observed, the profile curves are sharp changes, describing the phase difference (angle deflection) variation in proportion to the density variation (refractive index gradient) of the thermal plume in the test section. At the same time, the amplitude image of the thermal plume above the hot plate and the corresponding profile along a horizontal line are shown in

Fig.6c and Fig.6f, respectively. The brightness variation in the amplitude image represents the intensity variation of light. As seen in Fig.6c, the intensity variation of light passing through the thermal plume is not homogeneous. The image profile in Fig.6f confirms this result.

3.3. Thermal plume of the unstable candle flame

A candle was placed in the centre of the test section (referring to Fig.1). When the candle flame is absent, the camera captures a photograph of a reference image, as shown in Fig.7a. A mini fan slowly runs to allow the blown air in the test section, generating the unstable flame. In this condition, the camera captures an image distortion, as shown in Fig.7b. The appearance of fringe displacements in the image distortion indicates the presence of a thermal plume (hot air rising) above the unstable flame. The corresponding profiles, as shown in Fig.7c, along a vertical line (white dashed line) in Fig.7a and Fig.7b show the phase difference between both images. This result affirms that the thermal plume above the unstable candle flame modulates the phase of fringe patterns in the background plane.

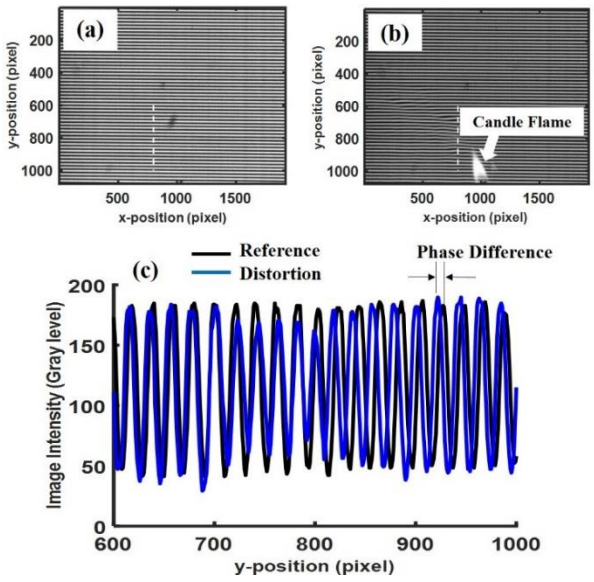

Fig. 7. Photograph of the background fringe patterns in the case of an unstable candle flame. (a) Reference image; (b) Image distortion due to the presence of an unstable candle flame in the test section; (c) The phase difference between both profiles of image intensity (in the gray level) along the white dashed line in both images (a) and (b).

The images, as shown in Fig.8a and Fig.8b, represent the phase and angle deflection images in the case of an unstable candle flame, respectively. Although the images tend to be dark, the contrast in both images can visually describe the presence of the thermal plume above the unstable candle flame in the test section. The brightness variation in both images describes the information on density variation (refractive index gradient) in the thermal plume. The corresponding image profiles along the white dashed line in the phase and angle deflection images support this result. As shown in Fig.8d and Fig.8e, the profile curves spatially fluctuate, describing the density variation or refractive index gradient of the thermal plume in the test section. Also, the amplitude image and the corresponding profile along a horizontal line are shown in Fig.8c and Fig.8f, respectively. Compared with the phase image (Fig.8a) or the angle deflection image (Fig.8b), the amplitude image (Fig.8c) appears more excellent in visualizing the thermal plume above the unstable candle flame. However, both images contain different physical information.

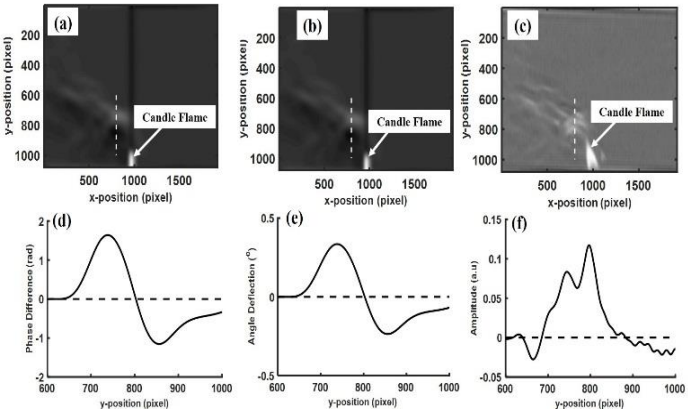

Fig. 8. The BOS visualization of the thermal plume in the case of a unstable candle flame: (a) Phase (phase difference) image; (b) Image of angle deflection; (c) Amplitude image; (d) Phase profile along the white dashed line in the image (a); (e) Angle deflection profile along the white dashed line in the image (b); and (f) Amplitude profile along the white dashed line in the image (c).

4. Conclusion

This paper presents a new way to visualize a thermal plume using the BOS technique based on the phase demodulation of fringe (periodic patterns) background, similar to the method used in the communication field. The background of the fringe pattern produces the spatial carrier frequency, and a phase object (transparent object) such as a wedge prism and thermal plume can modulate the fringe patterns into the phase modulation. The proposed BOS experimental has successfully demodulated the phase and reconstructed it into an image using the Hilbert Transform (HT). The calibration results show that the proposed BOS has accurately measured the angle deflection of light produced by a wedge prism. Finally, the calibrated BOS has successfully been used to visualize the thermal plume, a transparent gas invisible to the human eyes. In addition, this work produces the visualization of the thermal plume in the image of phase and amplitude. In future, the proposed BOS will be useful for visualizing and measuring the quantitative physical gas or other transparent material, such as the density distribution in industrial applications.

Acknowledgements

We would like to thank the Management of Metrology Laboratory, Ahmad Dahlan University for the financial and facilities supports. Special thanks addressed to Mr.Apik Rusdiarna IP from Study Program of Physics (Metrology - Materials Electronics-Instrumentation), Faculty of Science and Applied Technology (FAST), Ahmad Dahlan University, Yogyakarta, Indonesia for his sharing of knowledge and discussion on MATLAB programs and the use a CCD camera.

References

[1] A. W. Gena, C. Voelker, and G. S. Settles, “Qualitative and quantitative schlieren optical measurement of the human thermal plume,” *Indoor Air*, vol. 30, no. 4, pp. 757–766, 2020.

[2] G. Liu, Z. Jiang, and Q. Wang, “Analysis of gas leakage early warning system based on Kalman filter and optimized BP neural network,” *IEEE Access*, vol. 8, pp. 175180–175193, 2020.

[3] Q. Zhao, X. Nie, D. Luo, J. Wang, Q. Li, and W. Chen, “An Effective Method for Gas-Leak Area Detection and Gas Identification with Mid-Infrared Image,” *Photonics*, vol. 9, no. 12, 2022.

[4] A. M. Toscano, M. R. Lato, D. Fontanarosa, and M. G. De Giorgi, “Optical Diagnostics for Solid Rocket Plumes Characterization: A Review,” *Energies*, vol. 15, no. 4, 2022.

[5] M. C. Phillips, B. E. Bernacki, S. S. Harilal, J. Yeak, and R. J. Jones, “Standoff chemical plume detection in turbulent atmospheric conditions with a swept-wavelength external cavity quantum cascade laser,” *Opt. Express*, vol. 28, no. 5, p. 7408, 2020.

[6] K. McDonnell, L. Molnár, M. Harty, and F. Murphy, “Feasibility study of carbon dioxide plume geothermal systems in Germany−utilising carbon dioxide for energy,” *Energies*, vol. 13, no. 10, pp. 1–24, 2020.

[7] H. K. M. Tanaka *et al.*, “Atmospheric muography for imaging and monitoring tropic cyclones,” *Sci. Rep.*, vol. 12, no. 1, pp. 1–14, 2022.

[8] Y. Xiong, T. Kaufmann, and N. Noiray, “Towards robust BOS measurements for axisymmetric flows,” *Exp. Fluids*, vol. 61, no. 8, pp. 1–12, 2020.

[9] A. Moumen, J. Grossen, I. Ndindabahizi, J. Gallant, and P. Hendrick, “Visualization and analysis of muzzle flow fields using the Background-Oriented Schlieren technique,” *J. Vis.*, vol. 23, no. 3, pp. 409–423, 2020.

[10] J. T. Heineck, D. W. Banks, N. T. Smith, E. T. Schairer, P. S. Bean, and T. Robillos, “Background-oriented schlieren imaging of supersonic aircraft in flight,” *AIAA J.*, vol. 59, no. 1, pp. 11–21, 2021.

[11] Y. A. Barinov, “Features of the background oriented schlieren method for studying small axisymmetric plasma objects,” *J. Vis.*, vol. 24, no. 6, pp. 1131–1139, 2021.

[12] Q. Wang, J. Geng, P. Wang, F. Lv, and Y. Ding, “Measurement of discharge channel based on background oriented schlieren technique using an optimized algorithm,” *AIP Adv.*, vol. 11, no. 6, 2021.

[13] M. Meinecke, A. Kilzer, and E. Weidner, “Background Orientated Schlieren Method Applied for Liquid Systems of Strong Refractive Gradients,” *Chemie-Ingenieur-Technik*, vol. 92, no. 8, pp. 1089–1097, 2020.

[14] H. C. Liu, J. Q. Huang, L. Li, and W. W. Cai, “Volumetric imaging of flame refractive index, density, and temperature using background-oriented Schlieren tomography,” *Sci. China Technol. Sci.*, vol. 64, no. 1, pp. 98–110, 2021.

[15] T. Shimazaki, S. Ichihara, and Y. Tagawa, “Background oriented schlieren technique with fast Fourier demodulation for measuring large density-gradient fields of fluids,” *Exp. Therm. Fluid Sci.*, vol. 134, no. January, p. 110598, 2022.

[16] G. Li, J. Wu, K. Kontis, S. Wit, and Z. Fan, “Development of unsteady background-oriented schlieren system in an indraft supersonic wind tunnel,” *J. Phys. Conf. Ser.*, vol. 1786, no. 1, 2021.

[17] S. Wildeman, “Real-time quantitative Schlieren imaging by fast Fourier demodulation of a checkered backdrop,” *Exp. Fluids*, vol. 59, no. 6, p. 0, 2018.

[18] S. Sharma and R. Kulkarni, “Phase demodulation from a spatial carrier fringe pattern using extended complex Kalman filter,” *Opt. Lasers Eng.*, vol. 138, no. August 2020, p. 106409, 2021.

[19] H. Cai, Y. L. Wang, R. T. Wainner, N. V. Iftimia, C. V. Gabel, and S. H. Chung, “Wedge prism approach for simultaneous multichannel microscopy,” *Sci. Rep.*, vol. 9, no. 1, pp. 1–10, 2019.

[20] Y. Yang and C. Li, “Modulated signal detection method for fault diagnosis,” *IET Sci. Meas. Technol.*, vol. 14, no. 10, pp. 962–971, 2020.

[21] L. K. Rajendran, S. P. M. Bane, and P. P. Vlachos, “Uncertainty amplification due to density/refractive index gradients in background-oriented schlieren experiments,” *Exp. Fluids*, vol. 61, no. 6, pp. 1–16, 2020.

[22] J. E. Gómez-Correa, A. L. Padilla-Ortiz, A. Jaimes-Nájera, J. P. Trevino, and S. Chávez-Cerda, “Generalization of ray tracing in symmetric gradient-index media by Fermat’s ray invariants,” *Opt. Express*, vol. 29, no. 21, p. 33009, 2021.

[23] H. xin Zhang, X. Zhang, H. ran Qiu, and H. Zhou, “Automatic wavefront reconstruction on single interferogram with spatial carrier frequency using Fourier transform,” *Optoelectron. Lett.*, vol. 16, no. 1, pp. 75–80, 2020.

[24] D. Kaganovich, L. A. Johnson, A. A. Mamonau, and B. Hafizi, “Benchmarking background oriented schlieren against interferometric measurement using open source tools,” *Appl. Opt.*, vol. 59, no. 30, p. 9553, 2020.

[25] L. C. Wynne, H. T. Ballantyne, X. Li, A. Di Falco, and S. A. Schulz, “A Hilbert transform method for measuring linear and nonlinear phase shifts imparted by metasurfaces,” *Photonics Nanostructures - Fundam. Appl.*, vol. 42, p. 100844, 2020.

[26] Z. Wu, W. Guo, L. Lu, and Q. Zhang, “Generalized phase unwrapping method that avoids jump errors for fringe projection profilometry,” *Opt. Express*, vol. 29, no. 17, p. 27181, 2021.

[27] H. An, Y. Cao, H. Wu, N. Yang, C. Xu, and H. Li, “Spatial-temporal phase unwrapping algorithm for fringe projection profilometry,” *Opt. Express*, vol. 29, no. 13, p. 20657, 2021.